Fano Resonance-Plasmonic Biosensors Based on Strong Coupling of Hybrid Plasmonic-Photonic Modes

Kaifu Chen, Xingbing Li, Tianye Huang, Yuye Wang, Shuwen Zeng

Fano Resonance-Plasmonic Biosensors based on Strong Coupling of Hybrid Plasmonic-Photonic Modes

Kaifu Chen[1,†], Xingbing Li[4,†], Tianye Huang[1], Yuye Wang [2], Shuwen Zeng[3*]

[1] School of Mechanical Engineering and Electronic Information, China University of Geosciences(Wuhan), Wuhan 430074,China

* E-mails: 20211001031@cug.edu.cn(K.C.); huangty@cug.edu.cn(T.H.);

[2] State Key Laboratory of Radio Frequency Heterogeneous Integration, Key Laboratory of Optoelectronic Devices and Systems of Ministry of Education and Guangdong Province, College of Physics and Optoelectronics Engineering, Shenzhen University, Shenzhen, 518060, China

[3] Light, Nanomaterials & Nanotechnologies (L2n), CNRS-UMR 7076, Université de Technologie de Troyes, 10000 Troyes, France

* E-mails: shuwen.zeng@cnrs.fr

[4] School of Mathematics and Physics, China University of Geosciences(Wuhan), Wuhan 430074, China

* E-mails: bing@cug.edu.cn

† These authors contributed equally to this work.

Abstract:

Surface Plasmon Resonance (SPR) sensors are a useful tool for biomolecule detection, offering label-free and real-time monitoring characteristics. However, traditional SPR sensors still face the challenges of limited detection sensitivity, especially for sensing small molecules with a low concentration level (less than 1 pM (10^{-12} mol/L)). To overcome this challenge, in this paper, we designed a Kretschmann configuration which uses a plasmonic waveguide to generate a powerful Fano resonance through the coupling of the surface plasmon polariton (SPP) mode and photonic waveguide (PWG) mode at the sensing interface. By optimizing the thickness of the layers of the metamaterial structure, it is also possible to adjust the resonance angle, the reflectivity, the quality factor (Q factor), the intensity sensitivity, the angular sensitivity and the detection range. In our designed subwavelength grating waveguides (SWG) structure sensor, the intensity sensitivity reached 1.808×10^{4} RIU^{-1}, which surpassed the intensity sensitivity of uniform Si layers by 5.14 times. This approach provides a framework for physicists and biologists to develop the future generation of medical diagnostic devices.

1. Introduction

Early-stage diagnosis plays a crucial part in effectively preventing many diseases. Traditional early diagnostic methods include imaging, blood tests, genetic testing, and biopsies [1-4]. However, these conventional approaches have limitations such as long processing time, high cost, and insufficient accuracy [5]. To overcome these limitations, researchers have exploited optical biosensing schemes for early-stage disease diagnosis. Normally, the detection is based on the recognition of biomarkers in the samples collected from patients using optical biosensors [6]. Among these optical sensing technologies, surface plasmon resonance (SPR) biosensors show great potential due to their real-time and label-free detection characteristics [7]. However, traditional SPR sensors still face challenges in directly detecting analytes with extremely low concentrations (less than 1 pM) or small molecular weights (less than 400 Da), and they are prone to oxidation of the metal layer, which needs to be compensated by placing dielectric materials like silicon on its surface [8-11].

Recently, a new type of metamaterial biosensor, the Fano resonance (FR)-enhanced SPR sensor, has attracted a lot of attention [12-17]. These sensors integrate uniform waveguide layers into the well-known Kretschmann configuration. When two resonators have identical resonance, their destructive interference can form a narrow transparent window within a wide absorption band. However, when the frequency deviation between the wide and narrow resonances is sufficiently reduced, the perturbation between the two resonances results in a narrow transparent window at a broad transmission angle, generating a transmission peak similar to electromagnetically induced transparency (EIT). This asymmetric resonance peak is called the FR. The sharp peak-to-dip transition produced by FR in the spectrum allows for the detection of slight changes in sensing parameters, such as refractive index or temperature, by monitoring the change in the FR spectrum. Compared to other resonances like Lorentz resonances, FR possesses a higher Q factor, which greatly enhances detection sensitivity and selectivity [18-20]. By designing and adjusting the optical response of

the device, higher sensitivity can be achieved. Unlike traditional SPR sensors, which measure signals at the lowest reflection at the resonance angle, FR signals allow measurements to be made at higher reflectance. This advantage considerably improves the signal-to-noise ratio (i.e. resolution), a key factor in current rapid and accurate diagnostic procedures.

In addition to sensing resolution, a noteworthy measure is the detection sensitivity, which can be augmented through the design of SPR sensing substrates utilizing plasmonic metamaterials [21-25]. High sensitivity is crucial for detecting biomarkers with extremely low concentrations during the early stages of diseases [26,27]. Metamaterials are synthetic materials with electromagnetic properties not found in naturally occurring substances [28]. They can manipulate the phase, polarization, amplitude, and angle of incident light. The interaction between the measured material and confined electromagnetic waves in metamaterials at resonant frequencies enables plasmonic metamaterial sensors to achieve high sensitivity [30,31]. Subwavelength grating waveguides (SWG) refer to plate-like metamaterial structures characterized by dimensions smaller than the operating light wavelength. These waveguides effectively suppress diffraction effects, functioning as homogeneous plate waveguides with properties equivalent to birefringent materials [32]. SWG in uniform waveguides are fabricated with a single etching step in modern immersion lithography processes, providing a straightforward approach to alter the width, pitch, and duty cycle of gratings, which in turn allows for localized engineering of the effective refractive index, dispersion and mode size of the medium [33]. Therefore, SWG material structures are expected to provide an important basis for high-performance silicon optical devices and are suitable for mass production, with strong commercial potential [34-36].

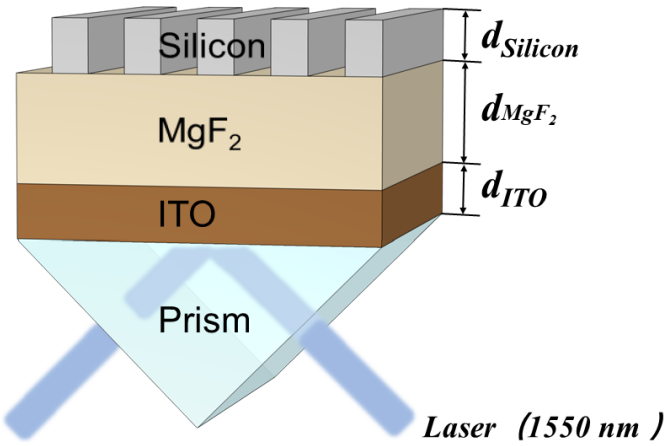

Figure 1. The configuration of the SPR sensor.

In this paper, we proposed a novel plasmonic metamaterial structure for SPR sensors, with the electric field mainly propagating between the MgF_2 thin film and the Si SWG on top as shown in Fig.1. In this configuration, ITO is utilized as the plasmonic material. This SPR sensor operates at a wavelength of 1550 nm in the infrared range. We conducted theoretical studies on improving the sensitivity of SPR using the Rigorous Coupled-Wave Analysis (RCWA) method. We first discussed the influence of the thickness of both Si and MgF_2 layers on the attenuated total reflection (ATR) curve and sensitivity. We also explored the relationship between the intensity sensitivity and detection range, demonstrating the advantage of combining SPR with FR. By modifying the spectrum of incident angles, a noteworthy improvement can be observed in both angular and intensity sensitivity. Additionally, the Si SWG for the proposed sensor can be made from uniform silicon waveguides on the MgF_2 substrate in only one etching step. They offer significant advantages in terms of the effective sensing area, sensitivity, and design freedom compared to the multilayer uniform structures proposed in previous work [12-17], offering great potential for improving the accuracy and detection time of early disease diagnosis.

2. Material and method

The proposed design combines an SPR sensor enhanced by Fano resonance [24,25] with a grating structured with grooves [37]. This device includes a rutile prism, a layer of ITO with a thickness of d_{ITO}, a layer of MgF_2 with a thickness of d_{MgF2}, and a grating

layer. The grating layer is a groove of silicon with a thickness of d_{Si} and is surrounded by water.

When the transverse magnetic (TM) wave at a wavelength of 1550 nm stimulates the surface plasmon polariton (SPP) mode and travels along the interface of ITO-MgF_2, the evanescent field of SPP intersects with the photonic waveguide (PWG) mode. This intersection causes a coupling between these two modes.

RCWA is a semi-analytical method used to solve the system of Maxwell's equations numerically [38,39]. It is widely used to accurately analyze electromagnetic diffraction in periodic structures. The method analyses a structure that consists of multiple uniform layers in the z-direction and periodic ridges and grooves in the x- and y-directions, corresponding to different refractive indices. TE (transverse electric) or TM (transverse magnetic) waves are incident from the x-z plane at a given polar angle. Maxwell's equations are used to calculate electromagnetic wave propagation within a layer, expressed as partial differential equations. Scattering matrices are used to match the boundary conditions for propagation at the layer boundary. The Floquet theory [40] expands Maxwell's equations and boundary conditions, with higher-order functions truncated for finite equations based on desired accuracy and convergence speed. The finite equations include structural parameters such as the thickness of each layer in the z-direction, the refractive index of the ridge and trench, and others. By adjusting these parameters, the computer can solve for the corresponding directional hemispherical reflectance and transmittance, and infer the absorptivity and emissivity.

The reflectivity and phase responses of the structure were modeled using the RCWA method. The structure consists of four layers. The initial layer involves the incident medium and a substrate with an infinite thickness, which possesses a refractive index of n_1. Uniform medium layers comprise the second and third layers. These two layers have defined thicknesses, d_2 and d_3, refractive indices n_2 and n_3. The fourth layer comprises gratings, which can be subdivided into ridges and grooves. Each has an accompanying refractive index of n_4. Furthermore, it is necessary to specify the height, period, filling ratio, and normalized position of the grating ridges within one period. An iterative method is used to adjust the structural parameters, considering the coupling of

the PWG mode and the SPP mode in the attenuated total reflection (ATR) curve stimulated using the RCWA method. The structure was studied for use with a 1550 nm laser. At this particular wavelength, the refractive indices of the rutile prism, MgF_2, Silicon, and ITO are 2.4532, 1.3705, 3.4777, and 0.2670 + 1.9123i, respectively [41-45].

3. Results and Discussion

To investigate the effect of d_{Si} on resonance peaks, ATR curves were calculated under the conditions of d_{ITO}=110 nm, d_{MgF2}=500 nm, and a Si layer with a grating structure having a period of 200 nm and a filling ratio of 0.5. The calculated ATR curve is shown in Fig.2. As the Si thickness increases, the resonance peak shifts towards larger incident angles. This is because the effective refractive index of the grating structure increases with increasing d_{Si} [46], requiring a larger incident angle for the coupling between the SPP mode and the PWG mode [47]. When d_{Si} increases from 500 nm to 800 nm, the full width at half maximum (FWHM) decreases noticeably. Furthermore, dips are observed at incident angles of 55.8770°, 63.6392°, 69.1414°, and 75.7996°, with corresponding reflectivity values of 0.0749, 0.1767, 0.3052, and 0.4770, respectively, indicating an approximate linearity which can give the proposed biosensor better flexibility in selecting operating parameters for practical use. The red ATR curve in Figure 2a displays a distinct peak of high reflectivity. This peak exhibits some resemblance to the behaviour observed in EIT systems. Points B and D in Figure 2a indicate the splitting of the initial single resonance angle into two separate angles. The EIT-like characteristics can be further elucidated by examining the distribution of electric field amplitude |E| at the reflection angles B and D, as well as the peak reflection denoted as C in Figures 2(b)-(d). Notably, the coupling of the SPP mode and the PWG mode occurs at these reflection angles, resulting in the excitation of a hybrid mode only when the incident light is at angles of 44.7062° and 49.8690°. Nevertheless, only the PWG mode is stimulated at the angle corresponding to the transparency peak (as shown in Figure 2(c)), leading to a significant suppression of absorption in the ITO layer. This

phenomenon bears similarity to the EIT effect observed in atomic systems, where the interference of two pathways results in the cancellation of bright modes. By utilizing the proposed method outlined in this study, precise control over light absorption and transmission can be achieved through adjustments in material structure and incident angle, thereby enabling the realization of EIT-like effects.

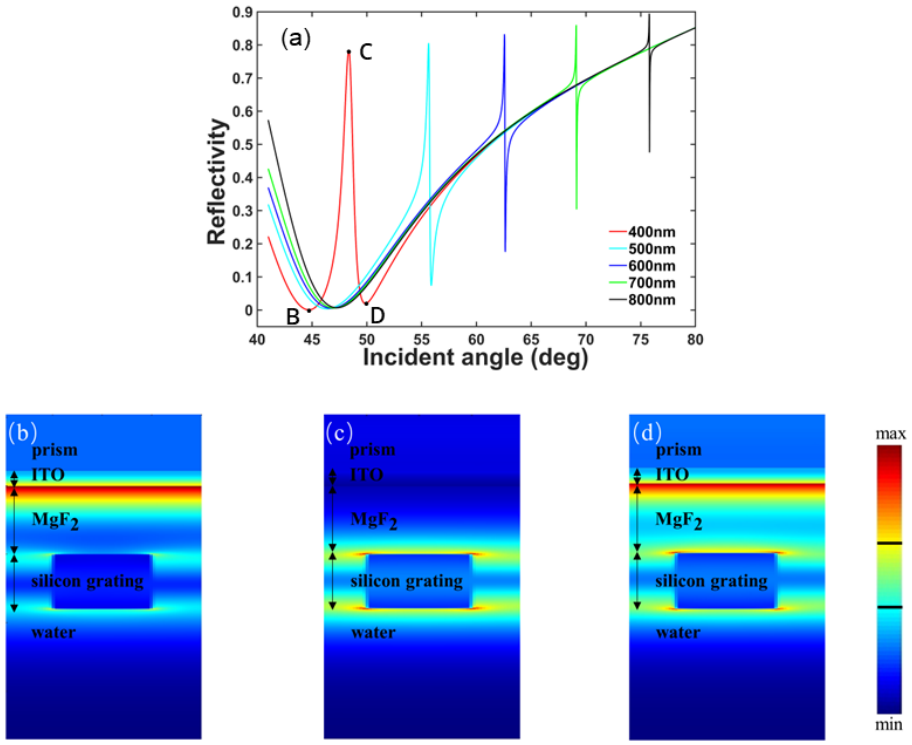

Figure 2. (a) Illustration of the influence of d_{Si} on the distribution of FR at the incident angle location. Results of the Rigorous Coupled-Wave Analysis (RCWA) method. d_{ITO}=110 nm, d_{MgF2}=500 nm, and the Si layer with a grating structure of a period of 200 nm and a filling ratio of 0.5, |E| distributions at point (b) B, (c) C, and (d)D simulated using Finite Difference Time Domain (FDTD).

In Fig.3, the differences (Δθ) between the FR peaks and valleys, as well as the Q factor, defined as the ratio between the resonance angle (θ) and the difference (Δθ) between the peaks and valleys of FR, is plotted. It can be observed that as the d_{Si} increases, the Q factor also increases. However, the Δθ decrease with increasing d_{Si}. This can also be clearly seen in Fig.2.

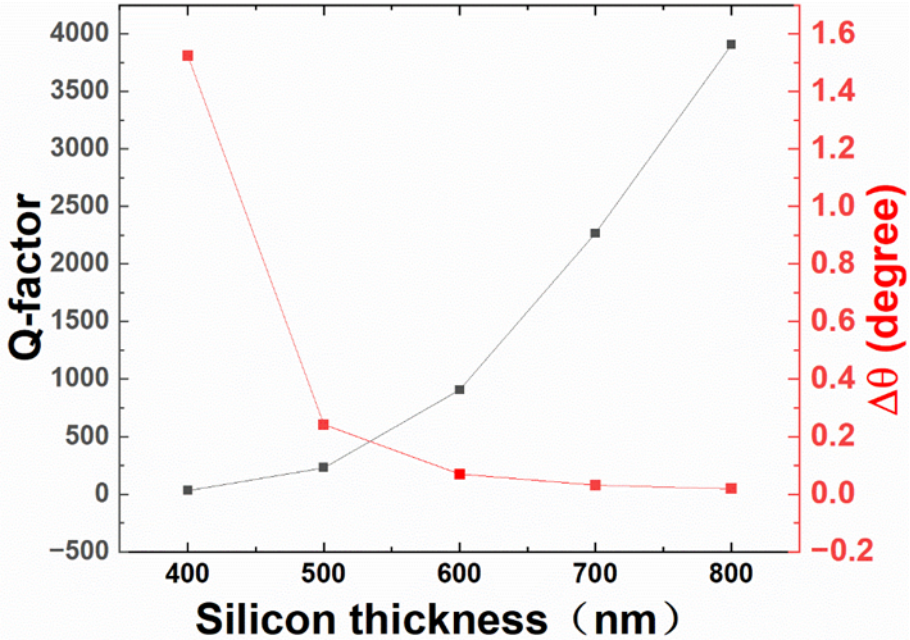

Figure 3. Q factor and Δθ versus d_{Si}. Results of the RCWA method. d_{ITO}=110 nm, d_{MgF2}=500 nm, and the Si layer with a grating structure of a period of 200 nm and a filling ratio of 0.5.

In Fig.4, we further investigated the influence of d_{Si} on intensity sensitivity and angular sensitivity. It can be observed that with an increase in d_{Si}, both intensity sensitivity and angular sensitivity exhibit a similar increasing trend. This indicates that increasing d_{Si} can enhance the sensor's sensitivity to intensity and incident angle.

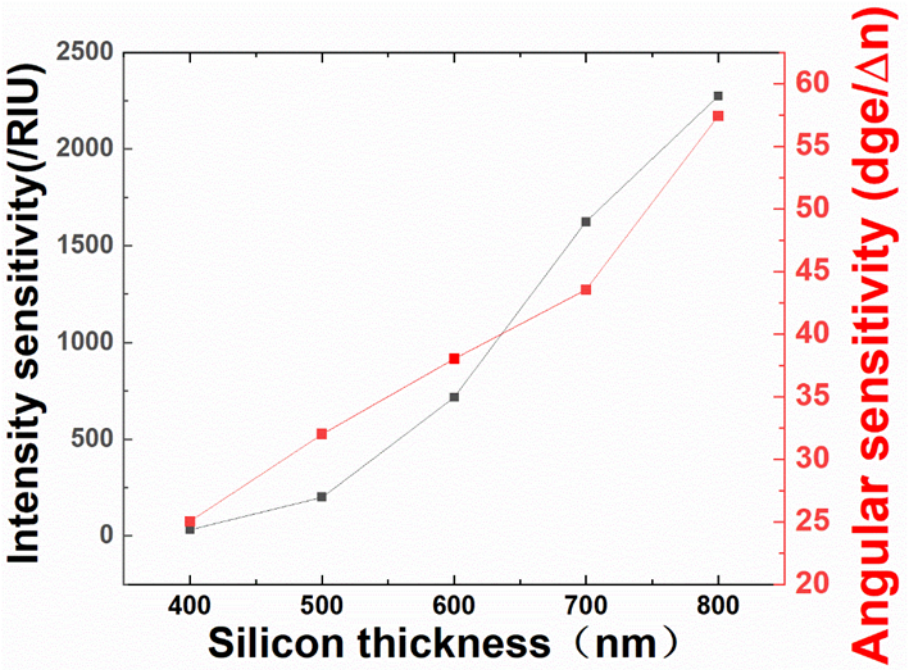

Figure 4. The intensity sensitivity and angular sensitivity versus d_{Si}. Results of the RCWA method.

d_{ITO}=110 nm, d_{MgF2}=500 nm, and the Si layer with a grating structure of a period of 200 nm and a filling ratio of 0.5.

To investigate the effect of MgF_2 layer thickness on the resonance peak, ATR curves were plotted for MgF_2 thickness ranging from 900 to 1400 nm under the conditions of ITO thickness of 110 nm, Si layer with a grating structure of 280 nm thickness, a period of 200 nm, and a filling ratio of 0.6. The resonance dip and resonance peak are located on the low-angle side and high-angle side, respectively. Furthermore, as the thickness of MgF_2 increases, the resonance dip shifts towards larger incident angles, while the resonance peak exhibits minimal movement and remains stable at approximately the same incident angle, as shown in Fig.5.

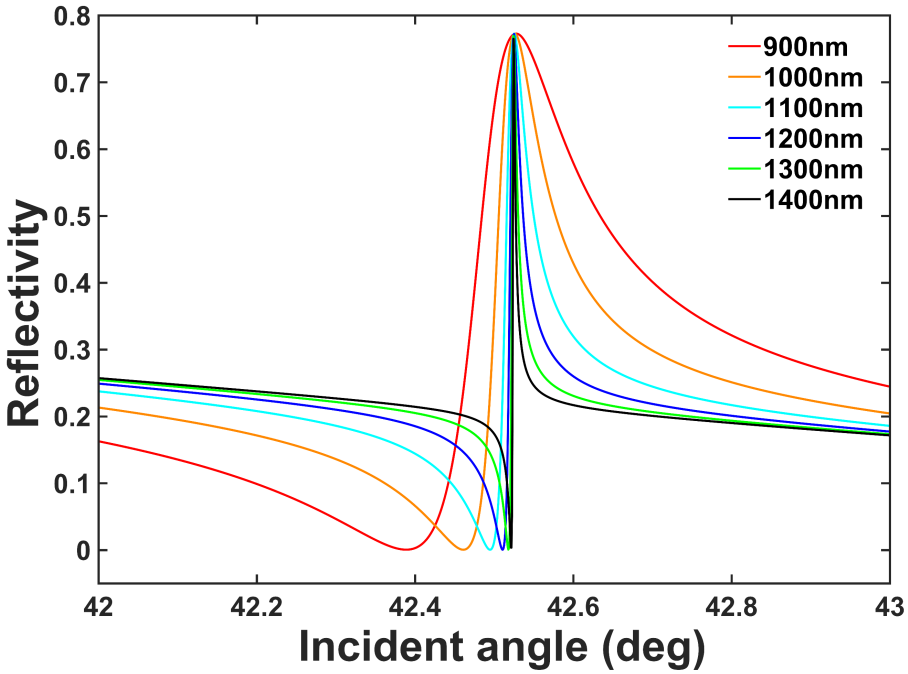

Figure 5. Illustration of the influence of MgF_2 thickness on the coupling strength to the SPR mode and PWG mode. Results of the RCWA method. d_{ITO}=110 nm, the Si layer with a grating structure of 280 nm thickness, a period of 200 nm, and a filling ratio of 0.6.

An increase in MgF_2 thickness led to a decreased coupling strength of the resonance peak, and vice versa [48]. Correspondingly, with the increased thickness of MgF_2, $\Delta\theta$ decreases with increasing MgF_2 thickness. Weakened coupling results in a

decrease in FWHM and generally leads to an increase in the Q-factor of FR, as shown in Fig.6.

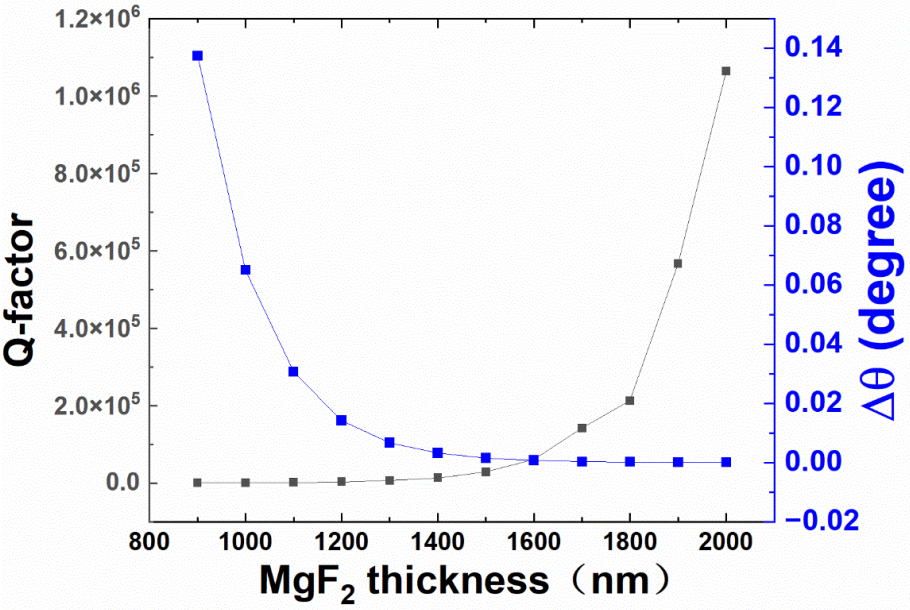

Figure 6. Q factor and Δθ versus MgF_2 thickness. Results of the RCWA method. d_{ITO}=110 nm, the Si layer with a grating structure of 280nm thickness, a period of 200nm, and a filling ratio of 0.6.

Regarding the angular and intensity sensitivity for this structure, as shown in Fig.7, it is found that the intensity sensitivity(The definition of intensity sensitivity is $\Delta R_n/\Delta n$, where ΔR_n refers to the change in reflectance when the refractive index of the material changes by Δn at the same angle in the linear region. In this study, we assumed that the refractive index of water can vary. We recorded the change in reflectance ΔR_n at the same incident angle in the linear region while varying the refractive index of water. Then, we compared this change in reflectance with the corresponding change in refractive index to obtain the intensity sensitivity.) increases continuously with the increase of MgF_2 layer thickness, without an upper limit or inflection point. In contrast to the case of increasing d_{Si}, the longitudinal distance between the peaks and valleys of the FR does not exhibit significant differences with increasing MgF_2 thickness. The angular sensitivity (The angle sensitivity is defined as $\Delta\theta_n/\Delta n$, where $\Delta\theta_n$ refers to the change in resonance angle when the refractive index of the material changes by Δn. In this study, we assume that the refractive index of water can vary. We record the resonance peak positions at different refractive indices of water, calculate the

displacement of the resonance peak $\Delta\theta_n$, and then compare it with the change in refractive index to obtain the angle sensitivity.) does not increase continuously like the intensity sensitivity but remains at 23.9°/RIU. This phenomenon occurs because changes in refractive index result in an overall shift of the resonance angle. However, increasing the MgF_2 thickness does not cause a shift in the resonance angle. Rather, it reduces the difference between the tilt angle and peak value ($\Delta\theta_d$), leading to an increased slope in the ATR curve. Consequently, under the condition of the same refractive index change and equal shift distance, the difference in values between the two corresponding curves increases. Theoretically, the strength sensitivity will continue to increase as the MgF_2 layer thickness increases. However, this results in a reduction of the detection range as the thickness increases. When the MgF_2 thickness reaches 1500 nm, the value of the detection range (defined as $\Delta\theta_d$/angle sensitivity) decreases to 6.3×10^{-5}, as shown in Fig.8.

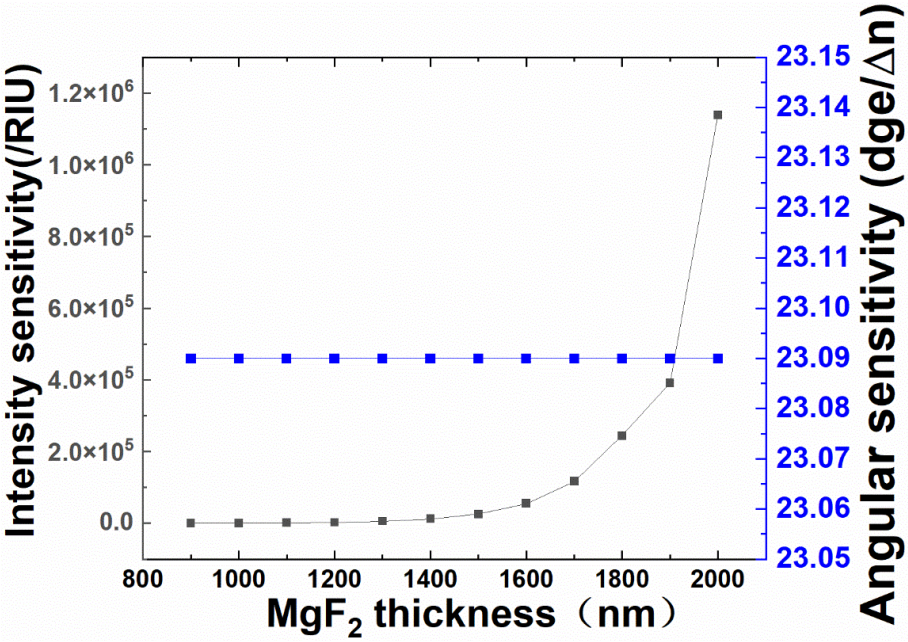

Figure 7. Intensity sensitivity and angular sensitivity versus MgF_2 thickness. Results of the RCWA method. d_{ITO}=110 nm, the Si layer with a grating structure of 280nm thickness, a period of 200 nm, and a filling ratio of 0.6.

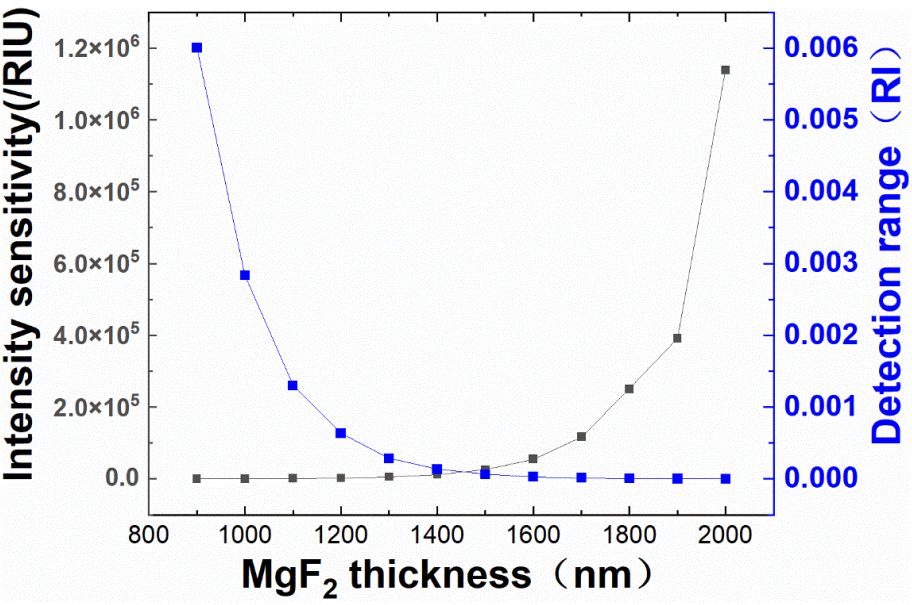

Figure 8. Intensity sensitivity and detection range versus MgF_2 thickness.

Results of the RCWA method. d_{ITO}=110 nm, the Si layer with a grating structure of 280nm thickness, a period of 200nm, and a filling ratio of 0.6.

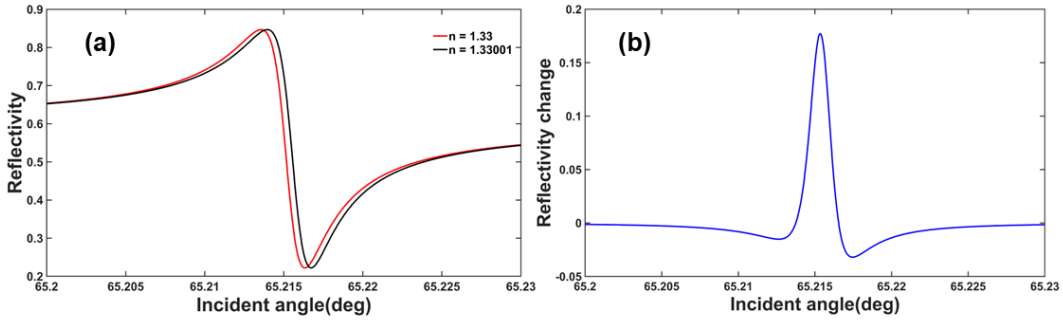

Figure 9. (a) Reflectivity versus the angle of incidence when the RI of the sample liquid is 1.33 and 1.33001, and (b) the corresponding change in reflectivity. Results of the RCWA method. d_{ITO}=110nm, d_{MgF2}=700 nm, the Si layer with a grating structure of 640nm thickness, a period of 200 nm, and a filling ratio of 0.6, The angle of incidence corresponding to the peak's top is 65.22°, demonstrating an intensity sensitivity of 1.808×10^4 RIU^{-1}.

Fig.9 illustrates the ATR curves for the sensing medium refractive indices of 1.33 and 1.33001, with Fig.9 (a) displaying the shift of the resonance peak towards larger incident angles as the refractive index increases. To investigate the sensing performance, the structural parameters were established as follows: d_{ITO}=110 nm, d_{MgF2}=700 nm, and

a Si layer comprising a grating structure with a thickness of 640 nm, a period of 200 nm, and a filling ratio of 0.5. The linear area between the steeply shifting peak top and bottom is appropriate for sensing monitoring. Fig.9 (b) depicts the change in reflectivity, with a corresponding incident angle at the peak top at 65.2153°, indicating a sensitivity of 1.808×10^4 RIU^{-1} based on intensity. When compared to the uniform silicon structure, the FR in the vicinity of 65°, which corresponds to an intensity sensitivity of 3.5×10^3 RIU^{-1} [13], the proposed grating-enhanced SPR sensor showed 5.14 times in intensity sensitivity higher than uniform Si layers. Furthermore, comparing the reflectance minima of the pure SPR dip close to 0, the reflectance minima of the dip of FR in Fig.9 are both 0.2222, thus allowing more power to be received. This enhancement is attributed to the enlarged contact area between the sensing medium and the grating structure when compared to the uniform structure.

4. Conclusion

In this study, we have developed an innovative SPR biosensor utilizing the surface-enhanced FR effect. We optimized the texture of the sensor substrate, including the thickness of the ITO layer, MgF_2 layer, and silicon layer. The filling ratio of the grating was also adjusted to achieve optimal performance. Through simulation analysis using the RCWA method, we optimized the parameters of the grating-enhanced sensing interface, with an ITO layer thickness of 110 nm, MgF_2 layer thickness of 700 nm, silicon layer thickness of 640 nm, a periodic structure of the super surface set at 200 nm, and a filling ratio of 0.5. It is also observed through simulation that the filling ratio of the MgF_2 layer grating structure has negligible effects on the overall sensitivity and resonance angle. In our designed grating structure sensor, the intensity sensitivity reached 1.808×10^4 RIU^{-1}, which is 5.14 times higher than the intensity sensitivity of 3.5×10^3 RIU^{-1} for conventional structures with uniform Si layers. The proposed grating-enhanced biosensor has broad prospects for early-stage diagnostics of various diseases.

References

[1] Zandoná, A. F., & Zero, D. T. (2006). Diagnostic tools for early caries detection.

The Journal of the American Dental Association, 137(12), 1675–1684. https://doi.org/10.14219/jada.archive.2006.0113.

[2] Chen, Q., He, Z., Mao, F., Pei, H., Cao, H., & Liu, X. (2020). Diagnostic Technologies for covid-19: A Review. RSC Advances, 10(58), 35257–35264. https://doi.org/10.1039/d0ra06445a.

[3] HARDING, A. E. (1981). Friedreich's ataxia: A clinical and genetic study of 90 families with an analysis of early diagnostic criteria and intrafamilial clustering of clinical features. Brain, 104(3), 589–620. https://doi.org/10.1093/brain/104.3.589.

[4] Bird-Lieberman, E. L., & Fitzgerald, R. C. (2009). Early diagnosis of Oesophageal Cancer. British Journal of Cancer, 101(1), 1–6. https://doi.org/10.1038/sj.bjc.6605126.

[5] Wang, L. (2017). Early diagnosis of breast cancer. Sensors, 17(7), 1572. https://doi.org/10.3390/s17071572.

[6] Wang, Y., Zeng, S., Crunteanu, A., Xie, Z., Humbert, G., Ma, L., Wei, Y., Brunel, A., Bessette, B., Orlianges, J.-C., Lalloué, F., Schmidt, O. G., Yu, N., & Ho, H.-P. (2021). Targeted sub-attomole cancer biomarker detection based on phase singularity 2D nanomaterial-enhanced plasmonic biosensor. Nano-Micro Letters, 13(1). https://doi.org/10.1007/s40820-021-00613-7.

[7] Wang, Z., Yu, M., Li, K., Mao, H., Liu, K., & Li, H. (2022). Tunable Fano resonance-enhanced surface plasmon biosensor based on MXene/mos2 heterostructure. Optical Materials, 133, 112966. https://doi.org/10.1016/j.optmat.2022.112966.

[8] Zeng, S., Baillargeat, D., Ho, H.-P., & Yong, K.-T. (2014). Nanomaterials enhanced surface plasmon resonance for biological and Chemical Sensing Applications. Chemical Society Reviews, 43(10), 3426. https://doi.org/10.1039/c3cs60479a.

[9] Law, W.-C., Yong, K.-T., Baev, A., & Prasad, P. N. (2011). Sensitivity improved surface plasmon resonance biosensor for cancer biomarker detection based on Plasmonic Enhancement. ACS Nano, 5(6), 4858–4864. https://doi.org/10.1021/nn2009485.

[10] Lee, K. S., Lee, M., Byun, K. M., & Lee, I. S. (2011). Surface plasmon resonance biosensing based on target-responsive mobility switch of magnetic nanoparticles under Magnetic Fields. Journal of Materials Chemistry, 21(13), 5156. https://doi.org/10.1039/c0jm03770b.

[11] Zhang, P., Wang, J., Chen, G., Shen, J., Li, C., & Tang, T. (2021). A high-sensitivity SPR sensor with bimetal/silicon/two-dimensional material structure: A theoretical analysis. Photonics, 8(7), 270. https://doi.org/10.3390/photonics8070270.

[12] S. Hayashi, D. V. Nesterenko, A. Rahmouni, Z. Sekkat. Observation of Fano line shapes arising from coupling between surface plasmon polariton and waveguide modes.

Appl. Phys. Lett. 1 February 2016; 108 (5): 051101. https://doi.org/10.1063/1.4940984.

[13] Huang, T., Zeng, S., Zhao, X., Cheng, Z., & Shum, P. (2018). Fano resonance enhanced surface plasmon resonance sensors operating in near-infrared. Photonics, 5(3), 23. https://doi.org/10.3390/photonics5030023.

[14] Zhu, J., Gan, S., Ruan, B., Wu, L., Cai, H., Dai, X., & Xiang, Y. (2018). Fano resonance in waveguide coupled surface exciton polaritons: Theory and application in Biosensor. Sensors, 18(12), 4437. https://doi.org/10.3390/s18124437.

[15] Yang, L., Wang, J., Yang, Lz. et al. Characteristics of multiple Fano resonances in waveguide-coupled surface plasmon resonance sensors based on waveguide theory. Sci Rep 8, 2560 (2018). https://doi.org/10.1038/s41598-018-20952-7.

[16] Bao, S., Jiang, H.D. & Zheng, G.G. Multiple Fano Resonances in Multilayer Thin Film-Coupled Attenuated Total Reflection Configuration. Plasmonics 16, 175–179 (2021). https://doi.org/10.1007/s11468-020-01281-w.

[17] A. Lotfiani, S.M. Mohseni, M. Ghanaatshoar, High-sensitive optoelectronic SPR biosensor based on Fano resonance in the integrated MIM junction and optical layers, Optics Communications, Volume 477,2020,126323,ISSN 0030-4018. https://doi.org/10.1016/j.optcom.2020.126323.

[18] Limonov, M. F. (2021). Fano resonance for applications. Advances in Optics and Photonics, 13(3), 703. https://doi.org/10.1364/aop.420731.

[19] Zhang, Y., Liu, W., Li, Z., Li, Z., Cheng, H., Chen, S., & Tian, J. (2018). High-quality-factor multiple Fano resonances for refractive index sensing. Optics Letters, 43(8), 1842. https://doi.org/10.1364/ol.43.001842.

[20] Baquedano, E., González, M. U., Paniagua-Domínguez, R., Sánchez-Gil, J. A., & Postigo, P. A. (2017). Low-cost and large-size nanoplasmonic sensor based on Fano resonances with fast response and high sensitivity. Optics Express, 25(14), 15967. https://doi.org/10.1364/oe.25.015967.

[21] Zeng, S., Sreekanth, K. V., Shang, J., Yu, T., Chen, C., Yin, F., Baillargeat, D., Coquet, P., Ho, H., Kabashin, A. V., & Yong, K. (2015). Graphene–gold metasurface architectures for ultrasensitive plasmonic biosensing. Advanced Materials, 27(40), 6163–6169. https://doi.org/10.1002/adma.201501754.

[22] Zeng, S., Hu, S., Xia, J., Anderson, T., Dinh, X.-Q., Meng, X.-M., Coquet, P., & Yong, K.-T. (2015). Graphene–mos2 hybrid nanostructures enhanced surface plasmon resonance biosensors. Sensors and Actuators B: Chemical, 207, 801–810. https://doi.org/10.1016/j.snb.2014.10.124.

[23] Jiang, L., Zeng, S., Xu, Z., Ouyang, Q., Zhang, D., Chong, P. H., Coquet, P., He, S., & Yong, K. (2017). Multifunctional hyperbolic nanogroove metasurface for

submolecular detection. Small, 13(30). https://doi.org/10.1002/smll.201700600.

[24] Oumekloul, Zakariae, Zeng, S., Achaoui, Y., Mir, A., & Akjouj, A. (2021). Multi-layer mos2-based plasmonic gold nanowires at near-perfect absorption for energy harvesting. Plasmonics, 16(5), 1613–1621. https://doi.org/10.1007/s11468-021-01405-w.

[25] Oumekloul, Z., Lahlali, S., Mir, A., & Akjouj, A. (2018). Evolution of LSPR of gold nanowire chain embedded in dielectric multilayers. Optical Materials, 86, 343–351. https://doi.org/10.1016/j.optmat.2018.10.020.

[26] Narlawar, S., Coudhury, S., & Gandhi, S. (2022). Magnetic properties-based biosensors for early detection of cancer. Biosensor Based Advanced Cancer Diagnostics, 165–178. https://doi.org/10.1016/b978-0-12-823424-2.00010-7.

[27] Mukherjee, S., & Das, S. (2022). Role of biosensor-based devices for diagnosis of Nononcological Disorders. Biosensor Based Advanced Cancer Diagnostics, 245–256. https://doi.org/10.1016/b978-0-12-823424-2.00020-x.

[28] Veselago, V. G. (1968). The electrodynamics of substances with simultaneously negative values of ϵ and μ. Soviet Physics Uspekhi, 10(4), 509–514. https://doi.org/10.1070/pu1968v010n04abeh003699.

[29] Yen, T. J., Padilla, W. J., Fang, N., Vier, D. C., Smith, D. R., Pendry, J. B., Basov, D. N., & Zhang, X. (2004). Terahertz magnetic response from artificial materials. Science, 303(5663), 1494–1496. https://doi.org/10.1126/science.1094025.

[30] Monticone, F., & Alù, A. (2017). Metamaterial, plasmonic and nanophotonic devices. Reports on Progress in Physics, 80(3), 036401. https://doi.org/10.1088/1361-6633/aa518f.

[31] Prakash, D., & Gupta, N. (2021). Applications of metamaterial sensors: A Review. International Journal of Microwave and Wireless Technologies, 14(1), 19–33. https://doi.org/10.1017/s1759078721000039.

[32] Schmid, J. H., Cheben, P., Janz, S., Lapointe, J., Post, E., Delâge, A., Densmore, A., Lamontagne, B., Waldron, P., & Xu, D.-X. (2008). Subwavelength grating structures in silicon-on-insulator waveguides. Advances in Optical Technologies, 2008, 1–8. https://doi.org/10.1155/2008/685489.

[33] Halir, R., Ortega-Monux, A., Benedikovic, D., Mashanovich, G. Z., Wanguemert-Perez, J. G., Schmid, J. H., Molina-Fernandez, I., & Cheben, P. (2018). Subwavelength-grating metamaterial structures for silicon photonic devices. Proceedings of the IEEE, 106(12), 2144–2157. https://doi.org/10.1109/jproc.2018.2851614.

[34] Przemek J. Bock, Pavel Cheben, Jens H. Schmid, Jean Lapointe, André Delâge, Siegfried Janz, Geof C. Aers, Dan-Xia Xu, Adam Densmore, and Trevor J. Hall,

"Subwavelength grating periodic structures in silicon-on-insulator: a new type of microphotonic waveguide," Opt. Express 18, 20251-20262 (2010). https://doi.org/10.1364/OE.18.020251.

[35] Wangüemert-Pérez, J. G., Hadij-ElHouati, A., Sánchez-Postigo, A., Leuermann, J., Xu, D. X., Cheben, P., ... & Molina-Fernández, Í. (2019). Subwavelength structures for silicon photonics biosensing. Optics & Laser Technology, 109, 437-448. https://doi.org/10.1016/j.optlastec.2018.07.071.

[36] C. M. Naraine, J. N. Westwood-Bachman, C. Horvath, M. Aktary, A. P. Knights, J. H. Schmid, P. Cheben, J. D. B. Bradley, Subwavelength Grating Metamaterial Waveguides and Ring Resonators on a Silicon Nitride Platform. *Laser Photonics Rev* 2023, 17, 2200216. https://doi.org/10.1002/lpor.202200216.

[37] Wangberg, R., Elser, J., Narimanov, E. E., & Podolskiy, V. A. (2006). Nonmagnetic nanocomposites for optical and infrared negative-refractive-index media. Journal of the Optical Society of America B, 23(3), 498. https://doi.org/10.1364/josab.23.000498.

[38] M. G. Moharam, Eric B. Grann, Drew A. Pommet, and T. K. Gaylord, "Formulation for stable and efficient implementation of the rigorous coupled-wave analysis of binary gratings," J. Opt. Soc. Am. A 12, 1068-1076 (1995). https://doi.org/10.1364/JOSAA.12.001068.

[39] Lifeng Li, "Use of Fourier series in the analysis of discontinuous periodic structures," J. Opt. Soc. Am. A 13, 1870-1876 (1996). https://doi.org/10.1364/JOSAA.13.001870.

[40] Kuchment, P. A. (1993). Floquet theory for partial differential equations (Vol. 60). Springer Science & Business Media.

[41] Ribarsky, M. W. (1997). Titanium dioxide (tio2) (rutile). Handbook of Optical Constants of Solids, 795–804. https://doi.org/10.1016/b978-012544415-6.50042-x.

[42] Singh, S., & Gupta, B. D. (2010). Simulation of a surface plasmon resonance-based fiber-optic sensor for gas sensing in visible range using films of nanocomposites. Measurement Science and Technology, 21(11), 115202. https://doi.org/10.1088/0957-0233/21/11/115202.

[43] Dodge, M. J. (1984). Refractive properties of magnesium fluoride. Applied Optics, 23(12), 1980. https://doi.org/10.1364/ao.23.001980.

[44] Tatian, B. (1984). Fitting refractive-index data with the sellmeier dispersion formula. Applied Optics, 23(24), 4477. https://doi.org/10.1364/ao.23.004477 .

[45] Segelstein, D. J. (1981). The complex refractive index of water.

[46] Kashyap, R. (2003). Why the χ(3) of silica increases after poling. Bragg Gratings, Photosensitivity, and Poling in Glass Waveguides. https://doi.org/10.1364/bgpp.2003.pd5.

[47] Islam, M. S., & Kouzani, A. Z. (2013). Variable incidence angle subwavelength grating SPR graphene biosensor. 2013 35th Annual International Conference of the IEEE Engineering in Medicine and Biology Society (EMBC). https://doi.org/10.1109/embc.2013.6610177.

[48] Wei, Y., Svedlindh, P., Kostylev, M., Ranjbar, M., Dumas, R. K., & Åkerman, J. (2015). Measuring acoustic mode resonance alone as a sensitive technique to extract antiferromagnetic coupling strength. Physical Review B, 92(6). https://doi.org/10.1103/physrevb.92.064418.